Excimer laser-induced crystallization of CdSe thin films

Etienne Shaffer · Amr S. Helmy · Dominique Drouin ·
Jan J. Dubowski

Abstract We have investigated ArF ($\lambda = 193$ nm) excimer laser-induced crystallization of amorphous CdSe semiconductor thin films. The crystallization has been monitored by a related photoluminescence emission in the free-exciton and defect-band transition regions. For different irradiation conditions, we have observed formation of nanorods, up to 2 μm long, as well as the formation of arrays of CdSe nanobeads with a narrow size distribution and characteristic dimensions corresponding to $\lambda/2$ and $\lambda/8$. The successful crystallization has also been confirmed by confocal Raman spectroscopy.

PACS 87.15.nt · 52.38.Mf · 78.55.-m · 78.67.Bf · 68.55.-a

1 Introduction

Semiconductor nanocrystals (NCs) and quantum dots (QDs) find many applications in photonics, e.g., for diode lasers [1], light emitting devices [2], photovoltaic cells [3], quantum computation [4], or as fluorescent labels [6]. They attract widespread interest due to their attractive physical properties leading to innovative optoelectronic devices [5] and emerging applications in biology and medicine [6–9].

E. Shaffer · D. Drouin · J.J. Dubowski (✉)
Department of Electrical and Computer Engineering, Université de Sherbrooke, 2500 boul. de l'Université, Sherbrooke, Québec J1K 2R1, Canada
e-mail: jan.j.dubowski@usherbrooke.ca

A.S. Helmy
The Edward S. Rogers, Sr. Department of Electrical and Computer Engineering, University of Toronto, 10 King's College Road, Toronto, Ontario M5S 3G4, Canada

Two-dimensional (2D) arrays of epitaxial quantum dots (eQDs) would allow for the spatially-resolved investigation of surface phenomena and QD-surface interactions. Such microstructures have been proposed as a promising platform for biosensing [10, 11]. The fabrication of 2D arrays of eQDs requires advanced epitaxial technologies, such as nanotemplate assisted chemical beam epitaxy [12], or state-of-the-art e-beam lithography [13]. Alternative approaches have reported spin coating of colloidal QDs (cQDs) on various substrates [14, 15], but due to the instability of cQDs outside of the solution and the requirement of special passivation procedures, they pose a significant challenge in the fabrication of reliable devices, and they are not well-suited for device integration. The crystallization of amorphous semiconductor thin films using lasers has been reported in the literature [16–18]. Due to their ability of delivering beams with power sufficient to melt thin films in defined spots, lasers have the potential to fabricate small 2D microcrystalline structures. In that context, the use of excimer lasers is especially attractive as they offer the capability of large area processing in relatively short times. For instance, excimer laser-induced crystallization (ELIC) of thin films is an industrial method used for the fabrication of Si thin film transistors (TFT) in flat panel displays [19]. A possible application of the ELIC technology to II–VI semiconductors has yet to be demonstrated. Here we report on the formation of 2D arrays of CdSe NCs induced by the irradiation of amorphous CdSe films with an ArF excimer laser ($\lambda = 193$ nm).

2 Experimental details

Samples were prepared for TFT devices as described in [20]. They consist of a n^+-Si$\langle 100 \rangle$ substrate on which a 300 nm-

Table 1 CdSe physical properties

	Name	Value
ρ	Average density (g cm^{-3})	5.7325 [21]
T_M	Melting temperature (°C)	1239 [21]
κ	Thermal conductivity (W cm^{-1} K^{-1})	0.09 [21]
c_T	Heat capacity at 300K (J g^{-1} K^{-1})	0.122 [22]
α	Absorption coef. at 193 nm (10^5 cm^{-1})	6.2 [23]
R	Reflection coef. at 193 nm	0.16 [23]

Fig. 1 Temperature depth profiles for a single-pulse laser irradiation, as calculated using the finite element method approximation. From bottom to top are the profiles for $F = 25$, 50, 75, and 100 mJ cm^{-2}, at the moment when the surface temperature was at its maximum

thick thermal gate oxide was grown. The 85 nm-thick film of amorphous CdSe was thereafter deposited by evaporation at 70°C from a 99.995% pure CdSe source. X-ray diffraction (XRD) and scanning electron microscopy (SEM) showed that samples were of an amorphous nature, with an average grain size of about 30–40 nm.

The irradiation was carried out in an air environment using an excimer laser *GSI Lumonics Pulsemaster PM-800* filled with a standard recipe of ArF gas mixture. Laser beam was homogenized by a *fly-eye* array comprising 36 cylindrical lenses. The irradiation was realized with a mask projection system having a demagnification ratio of approximately 1:3. The laser pulse rate was 2 Hz and the pulse full width at half maximum (FWHM) was 12 ns. The exact pulse waveform, as collected by a photodiode, was used to model the laser-induced temperature in our heat transfer simulations based on the Finite Element Method (FEM) approximation.

Low-temperature photoluminescence (PL) (20K) was excited with a frequency doubled Nd:YAG laser ($\lambda = 532$ nm). The laser scattered light was filtered out and the PL signal was dispersed by a monochromator and detected by a photomultiplier.

Confocal Raman spectroscopy measurements were carried out at room temperature with a *Jobin Yvon Horiba LabRAM* micro-Raman system using a CW 532 nm doubled Nd:YAG laser as an excitation source. The laser beam was directed into the system with a pair of two-axis adjustable mirrors, and a single lens and two apertures were used to assist in alignment outside the system. A confocal aperture was located between the collection optics and the spectrometer and it was adjustable from 0 to 1500 μm. The measurements were carried out with a 1.8 mW exciting laser beam focused through a 100× objective, a 100 μm slit and a 100 μm confocal aperture. A 5 second accumulation time was used, and each spectrum represents an average of 10 subsequent measurements.

The X-ray analysis was carried out using a *Zeiss Supra 55* SEM equipped with a field emission electron source and an *Oxford Instrument* energy dispersive X-ray (EDX) spectroscopy detector. This setup is capable of producing a nanometer scale probe size at low electron energy (<6 keV).
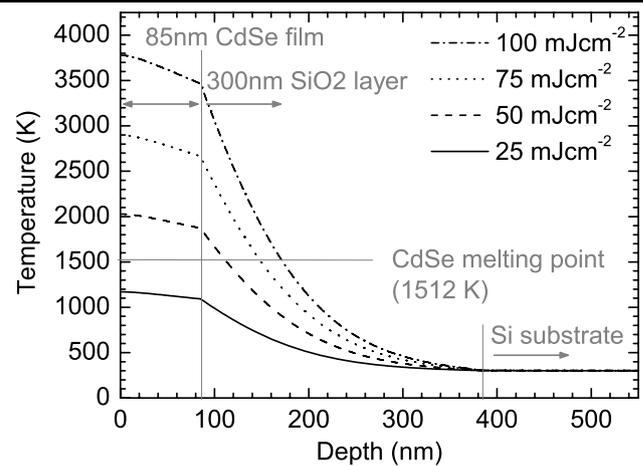
3 Results and discussion

3.1 Heat transfer modeling

For a laser beam that is spatially homogeneous in the XY-plane of the sample, the heat transfer can be treated as a one-dimensional (1D) problem along the depth (Z) of the sample. Such an approximation is valid as long as the XY in-plane coordinates are far enough from the irradiated edges, i.e., where the temperature profiles can not be noticeably affected by the heat sink from the non-irradiated region. Both CdSe and SiO$_2$ are relatively efficient thermal insulators; thus, the transition region where the temperature depth profiles are position-dependent is quite small. We have observed no visible change in the temperature depth profiles at 5 μm away from the border with the non-irradiated region.

Heat propagation in the sample was modeled in 1D using the FEM approximation to solve the following equation:

$$\rho C_P \left(\frac{\partial T}{\partial t} \right) = \frac{\partial}{\partial x} \left(\kappa \frac{\partial T}{\partial x} \right) + Q, \qquad (1)$$

where Q is the heat source per unit of volume [W cm^{-3}], κ is the thermal conductivity [W cm^{-1} K^{-1}], T is the temperature [K], ρ is the material density [g cm^{-3}] and t is time [s]. The laser pulse waveform was fitted numerically and used to reproduce the temporal dependence of the heat source. In agreement with experimental observation, PL emission from amorphous CdSe was considered negligible, and thus the entire energy of the irradiating laser contributed to the heating only. We used the simplified boundary condition:

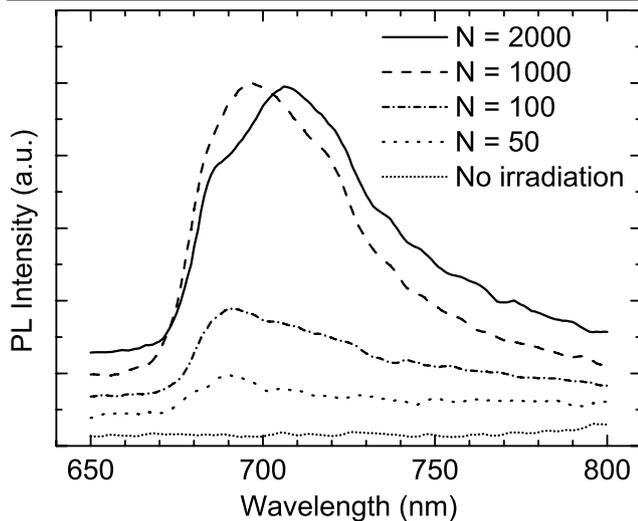$$q_0 - \sigma \epsilon \left(T_{amb}^4 - T^4 \right) = \kappa \Delta T, \qquad (2)$$

Fig. 2 Low-temperature (20 K) photoluminescence spectra from as-grown (amorphous) CdSe material and samples subjected to laser irradiation at a fluence of $50 \, \text{mJ cm}^{-2}$ for different number of pulses (N)

Fig. 3 Confocal Raman spectra from as-grown material (*dotted line*) and the 50-pulse laser irradiated sample at $50 \, \text{mJ cm}^{-2}$

that takes only diffusion and radiation into account. Convection has been omitted since it plays no significant role in the heat transfer dynamic of our system. In (2), q_0 is the entering heat flux [W cm^{-2}], σ is the Boltzmann constant [J K^{-1}] and ϵ is the emissivity. For CdSe, we have assumed material phase and temperature-independent physical properties as reported in the Table 1. For Si and SiO$_2$, the temperature-dependent parameters are well documented and already implemented in the FEM software. For amorphous CdSe, we used an averaged density of the CdSe *wurtzite* and *zincblende* structures. All other physical properties are assumed to be isotropic and emissivity was arbitrarily set to unity. It is interesting to note that absorption and reflection coefficients of Si and SiO$_2$ have no influence on the results since laser radiation is absorbed entirely in the CdSe film (absorption depth ≈ 16 nm). Simulated temperature depth profiles are presented in Fig. 1 for a single pulse laser irradiation and laser fluences of 25, 50, 75, and $100 \, \text{mJ cm}^{-2}$. It can be seen that the SiO$_2$ layer provides a relatively efficient thermal isolator allowing the entire CdSe film to reach the melting temperature for $F = 50 \, \text{mJ cm}^{-2}$. We found that no significant heat accumulation effect occurs for multiple laser pulses irradiation, as long as the laser pulse repetition rate is below 1000 Hz.

3.2 Thin films crystallization

Figure 2 shows a series of PL spectra collected at 20 K from as-grown material and samples that were irradiated with different number of pulses at $F = 50 \, \text{mJ cm}^{-2}$. No PL signal could be observed from the as-grown sample. However, a free-exciton peak located at near 683 nm appears for a sample irradiated with 50 pulses. The intensity
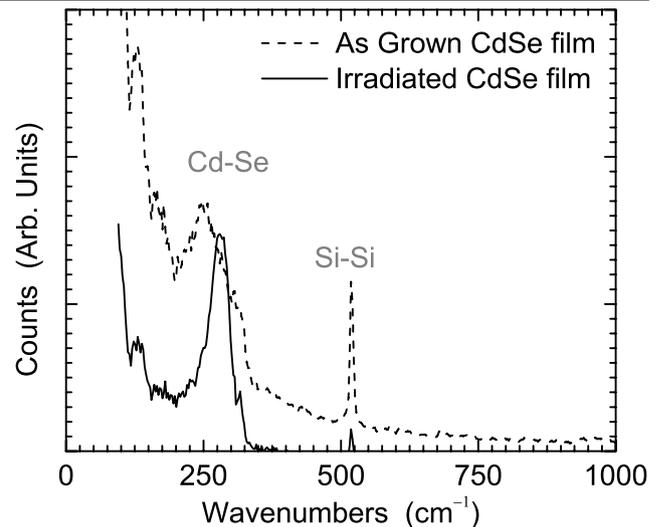
of this peak systematically increases with increasing number of pulses, up to $N = 1000$ pulses. For the sample irradiated with 2000 pulses, only a weak shoulder is observed near 683 nm. The entire PL spectrum is dominated by a peak located near 707 nm. This feature is likely associated with a donor–acceptor transition that has been observed in CdSe [24]. It is expected that some of the CdSe material is ablated with a 193 nm laser delivering $50 \, \text{mJ cm}^{-2}$ pulses. For instance, ablation of CdTe, a II–VI semiconductor very similar to CdSe, has been reported at 0.4 nm per pulse in vacuum for a 248 nm excimer laser operating at similar fluence [25]. Therefore, the donor–acceptor transition observed in Fig. 2 could be due to the decomposition of the material irradiated in the air environment and/or formation of surface defects.

Confocal Raman spectra for as-grown CdSe and a sample irradiated with 50 pulses at $50 \, \text{mJ cm}^{-2}$ are shown in Fig. 3. A sharp Si–Si peak at 524 cm^{-1} and a weak broad feature centered around 250 cm^{-1} originating form the CdSe film are easily resolvable in this figure. This agrees well with previous reports for CdSe amorphous layers [26]. The broad feature is made out of several peaks. On the smaller wavenumber side lies the LO phonon mode of CdSe (220 cm^{-1}), while on the larger wavenumber side lies the multi-phonon modes [27]. A significant increase of the intensity of this feature, as compared to the Si–Si related peak is observed in the irradiated samples, which is also accompanied with substantial reduction in its FWHM. This is a strong evidence of the formation of a crystalline phase of the CdSe material upon excimer laser irradiation. A peak originating from multi-phonon modes of LO+TA and TO+LA peaks in the 260–280 cm^{-1} region of crystalline CdSe [27] is clearly identifiable in that figure.
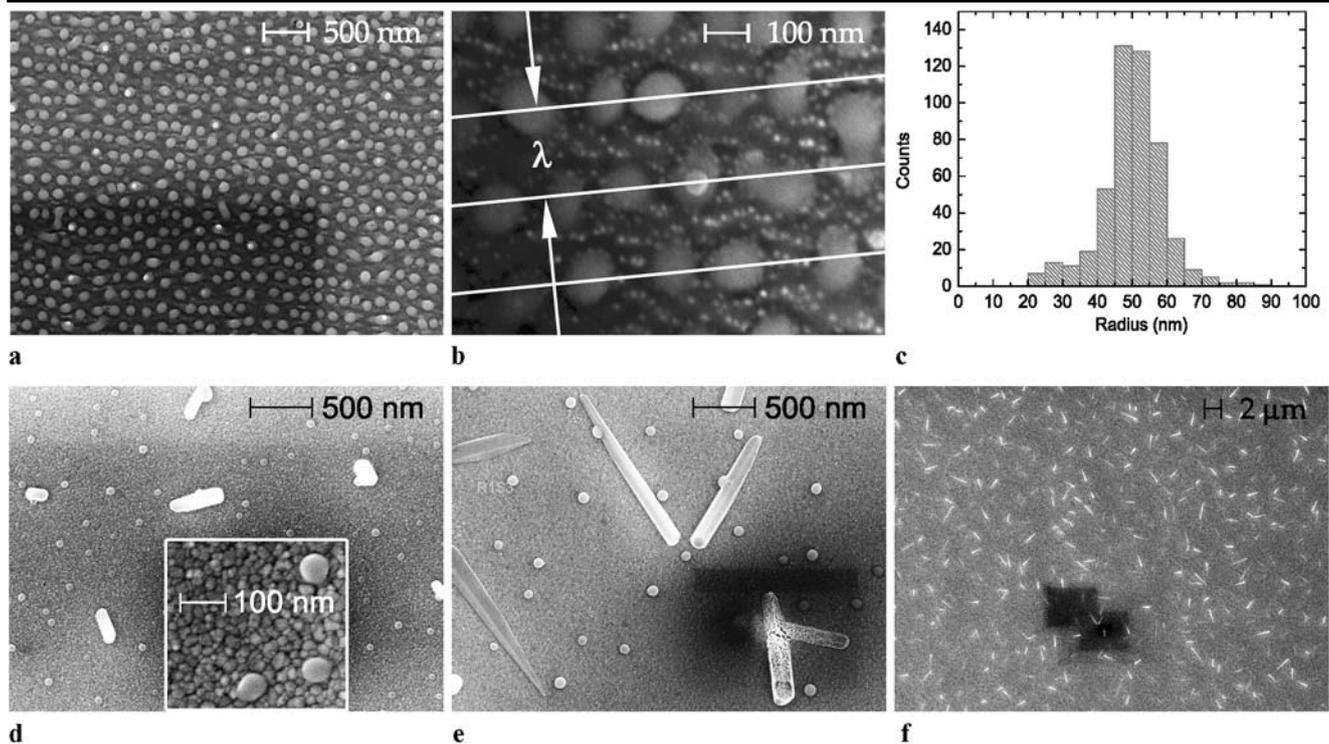
Fig. 4 Scanning electron micrograph (SEM) of the CdSe film irradiated by an ArF excimer laser with 1000 pulses at 25 mJ cm^{-2} (**a**). The spacing between two adjacent lines of organized nanobeads is equal to λ (**b**), and the nanobead average diameter corresponds to $\lambda/2$ (**c**). Nanorods grown from CdSe films irradiated with 50 (**d**) and 250 (**e**) pulses at 25 mJ cm^{-2}: crystallographic facets are visible, especially for nanorods in the periphery of the field of view. An array of randomly organized nanorods (250 pulses, 25 mJ cm^{-2}) is shown by a low-magnification micrograph (**f**)

3.3 Nanostructures formation

The formation of small microstructures has been observed for the films irradiated with $F = 25$ mJ cm^{-2}, i.e., at the fluence insufficient to melt the investigated CdSe films. A dedicated experiment (the results not shown here) has indicated a growing crystallinity of such films, up to the irradiation with 2000 pulses, although their PL free-exciton emission peak could not be resolved from the broad feature observed at near 700 nm. For 4000 pulses, the intensity of this feature has significantly decreased. It is reasonable to expect that this decrease is due to the laser-induced ablation. Figures 4(a), 4(b), and 4(c) show SEM micrographs of nanobeads obtained following the irradiation with 1000 pulses at 25 mJ cm^{-2}. It can be seen that the spacing between two adjacent lines of organized nanobeads is equal to λ (Fig. 4(b)), and the nanobead average diameter corresponds to $\lambda/2$ (Fig. 4(c)). Also visible in Fig. 4(b) are approximately 4–5 times smaller nanobeads organized in the vicinity of the 100 nm diameter objects. Their size distribution seems quite narrow, but the resolution of the SEM images did not allow for quantitative analysis of this parameter. The presence of these nanobeads suggests that the ELIC technique could be used to fabricate

CdSe nanocrystals demonstrating optical quantum confinement effects.

Due to the laser scattering effects at the irradiated surface, the distribution of laser beam intensity could be strongly nonuniform on the wavelength, or a fraction of the wavelength scale. The interference pattern between the incident and the surface-scattered electric fields give rise to local energy density maxima where the ablation of material could take place. This phenomenon, known as laser-induced periodic surface structures (LIPSS) and first reported in 1965 by Birnbaum et al. [28] is likely responsible for the formation of nanostructures observed in this work.

Note that somewhat similar although less organized and much larger nanostructures have been previously observed by Pal et al. [29] for CdSe irradiated with an unfocused beam of a multimode Ar-ion laser.

For samples irradiated with low number of pulses at 25 mJ cm^{-2}, we have observed the growth of nanorods, up to 2 μm long, with clearly visible crystallographic facets. This is illustrated in Figs. 4(d) and 4(e) which show CdSe films irradiated with 50 and 250 pulses, respectively. An array of randomly organized nanorods obtained with 250 pulses at 25 mJ cm^{-2} is shown by a low-magnification micrograph in Fig. 4(f).
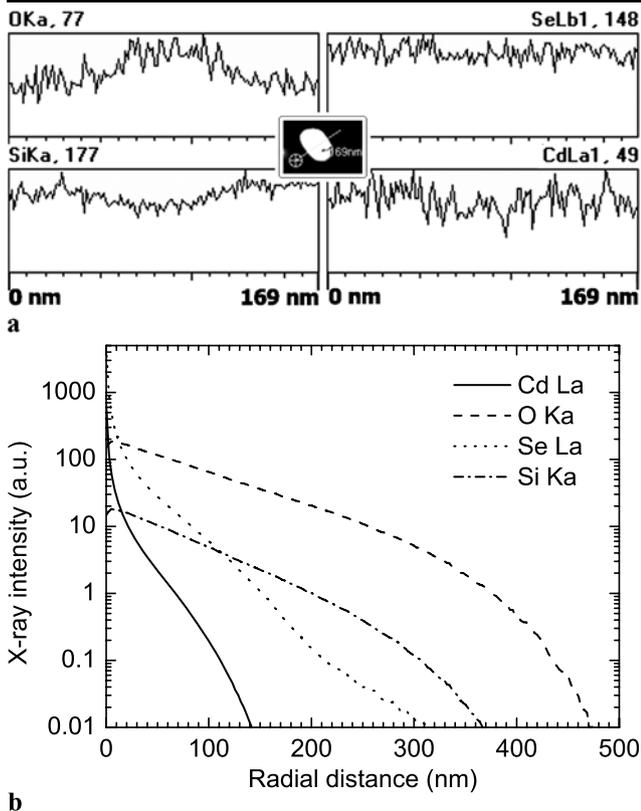
a

b

Fig. 5 Scanning electron micrograph (SEM) and energy dispersive X-ray (EDX) analysis of a 100 nm wide CdSe nanobead obtained following the irradiation with 1000 pulses at 25 mJ cm^{-2}. Maximum values of X-ray intensities (count) for each of the investigated elements are shown next to their respective symbols (Y scale is linear and its origin is at zero) (**a**). Monte Carlo simulation of the relative contribution to each EDX peak intensity in relation with the radial distance from the analyzed spot (**b**)

Composition of individual nanobeads was studied using an EDX analysis. Figure 5(a) shows relative concentrations of oxygen, silicon, selenium, and cadmium measured across a slightly elongated nanobead of which a SEM picture is included in the center of that figure. From the SeLb1, 148 and CdLa1, 49 profiles of Fig. 5(a), and since the in-depth sensibility for these two materials is very high, we can conclude that there is at least a very thin layer formed of Cd and Se everywhere, i.e., both the bead and the background. The drop in the SiKa, 177 signal allows us to believe that (1) the bead is not formed of silicon and (2) it lies on top of the surface; therefore, screening the SiKa, 177 signal from below. Finally, the increase in the OKa, 77 signal over the bead surface is a sign that it is partly composed of Cd–O and/or Se–O; however, it is impossible to estimate to what extent. Such contamination is expected given the atmospheric environment in which the laser irradiation took place. We note that the presence of oxide in CdSe has been attributed to the donor–acceptor

peak observed in the PL spectrum [30]. The reduced EDX Si signal is likely related to the increased screening of the SiO$_2$ layer by the fabricated nanobead. Figure 5(b) presents Monte Carlo simulations [31] of the relative contribution to the peak intensity of Si, O, Cd, and Se at 6 keV as a function of the distance from the analyzed spot. It demonstrates that the X-ray emission intensities decrease drastically within 140 and 310 nm for Cd and Se, respectively. This compares with 370 and 470 nm for Si and O, respectively. Thus, the concentration of Cd and Se has been estimated with a relatively better in-depth resolution than that of Si and O.

4 Conclusion

We have investigated ArF ($\lambda = 193$ nm) excimer laser induced crystallization (ELIC) of amorphous CdSe films deposited on a thin layer of native oxide (SiO$_2$) of a Si substrate. A finite element method (FEM) was implemented to model the laser-induced heat transfer in the irradiated microstructures. The photoluminescence measurements have indicated the formation of a crystalline phase in samples irradiated with pulses at 50 and 25 mJ cm^{-2}. Photoluminescence free-exciton and donor–acceptor transitions have been identified in such films. However, only limited crystallization could be achieved in films irradiated with pulses at 25 mJ cm^{-2}. Confocal Raman spectroscopy measurements provided strong evidence of the formation of a crystalline phase of the CdSe material upon excimer laser irradiation. Scanning electron microscopy study has revealed the formation of up to 2 μm long CdSe nanorods of dimensions smaller than 100 nm at the base. Crystallographic facets that have been observed for some of the nanorods confirm that, indeed, the crystallization process takes place in the laser-induced films. Arrays of small nanobeads, less than 20 nm diameter, have been observed for samples irradiated with a large number of pulses at the below-the-melting temperature fluence of 25 mJ cm^{-2}. A strongly non-uniform distribution of the laser beam intensity at the irradiated surface that leads to the formation of laser-induced periodic surface structures is a mechanism likely responsible for the formation of nanobeads. It is expected that following the optimization procedure, 2D arrays of even smaller nanobeads, such as those exhibiting optical quantum confinement effects could be fabricated with the ELIC technique.

References

1. N.N. Ledentsov, M. Grundmann, F. Heinrichsdorff, D. Bimberg, V.M. Ustinov, A.E. Zhukov, M.V. Maximov, Z.I. Alferov, J.A. Lott, IEEE J. Select. Topics Quantum Electron. **6**, 439 (2000)
2. A.D. Yoffe, Adv. Phys. **50**, 1 (2001)
3. A.J. Nozik, Physica E **14**, 115 (2002)
4. D. Loss, D.P. DiVincenzo, Phys. Rev. A **57**, 57 (1998)
5. P. Bhattacharya, S. Ghosh, A.D. Stiff-Roberts, Annu. Rev. Mater. Res. **34**, 1 (2004)
6. M. Bruchez, M. Moronne, P. Gin, S. Weiss, A.P. Alivisatos, Science **281**, 2013 (1998)
7. A.P. Alivisatos, Nat. Biotechnol. **22**, 47 (2004)
8. S. Kim, Y.T. Lim, E.G. Soltesz, A.M. De Grand, J. Lee, A. Nakayama, J.A. Parker, T. Mihaljevic, R.G. Laurence, D.M. Dor, L.H. Cohn, M.G. Bawendi, J.V. Frangioni, Nat. Biotechnol. **22**, 93 (2004)
9. W.J. Parak, D. Gerion, T. Pellegrino, D. Zanchet, C. Micheel, S.C. Williams, R. Boudreau, M.A. Le Gros, C.A. Larabell, A.P. Alivisatos, Nanotechnology **14**, R15 (2003)
10. J.J. Dubowski, S. Tanev, *Photon-based Nanoscience and Nanobiotechnology*. NATO Science Series II: Mathematics and Chemistry (Springer, New York, 2006), p. 159
11. X. Ding, Kh. Moumanis, J.J. Dubowski, E. Frost, E. Escher, Appl. Phys. A **83**, 357 (2006)
12. R.L. Williams, G.C. Aers, J. Lefebvre, P.J. Poole, D. Chithrani, Physica E **13**, 1200 (2002)
13. Y.W. Su, C.S. Wu, C.C. Chen, C.D. Chen, Adv. Mater. **15**, 49 (2003)
14. H.J. Choi, J.K. Yang, S. Yoon, H.H. Park, Appl. Surf. Sci. **244**, 92 (2002)
15. W. Marx, D.S. Ginger, K. Walzer, K. Stokbro, N.C. Greenham, Nano Lett. **2**, 911 (2002)
16. J.S. Im, H.J. Kim, M.O. Thompson, Appl. Phys. Lett. **63**, 1969 (1993)
17. Y.C. Peng, G.S. Fu, W. Yu, S.Q. Li, Y.L. Wang, Semicond. Sci. Technol. **19**, 759 (2004)
18. M. Mulato, D. Toet, G. Aichmayr, P.V. Santos, I. Chambouleyron, Appl. Phys. Lett. **70**, 3570 (1997)
19. S.D. Brotherton, Semicond. Sci. Technol. **10**, 721 (1995)
20. M.J. Deen, S.L. Rumyantsev, D. Landheer, D.-X. Xu, Appl. Phys. Lett. **77**, 2234 (2000)
21. O. Oda, *Compound Semiconductor Bulk Materials and Characterization* (World Scientific, Singapore, 2007), p. 371
22. F. Benkabou, H. Aourag, M. Certier, Mater. Chem. Phys. **66**, 10 (2000)
23. M. Cardona, G. Harbeke, Phys. Rev. **137**, A1467 (1965)
24. R. Jäger-Waldau, N. Stücheli, M. Braun, M. Lux Steiner, E. Bucher, R. Tenne, H. Flaisher, W. Kerfin, R. Braun, W. Koschel, J. Appl. Phys. **64**, 2601 (1988)
25. P.D. Brewer, J.J. Zinck, G.L. Olson, Appl. Phys. Lett. **57**, 2526 (1990)
26. D. Nesheva, I.P. Kotsalas, C. Raptis, E. Vateva, J. Noncryst. Solids **224**, 283 (1998)
27. R. Geick, C.H. Perry, S.S. Mitra, J. Appl. Phys. **37**, 1994–1997 (1966)
28. M. Birnbaum, J. Appl. Phys. **36**, 3688 (1965)
29. U. Pal, S. Munoz-Avila, L. Prado-Gonzalez, R. Silva-Gonzalez, J.M. Gracia-Jimenez, Thin Solid Films **381**, 155 (2001)
30. M.J.S.P. Brasil, P. Motisuke, F. Decker, J.R. Moro, J. Phys. C: Solid State Phys. **21**, 3141 (1987)
31. D. Drouin, A.R. Couture, D. Joly, X. Tastet, V. Aimez, R. Gauvin, Scanning **29**, 92 (2007)